22 Nair, R R, Ittekkot, V, Manganini, S, Ramaswamy, V., Haake, B, Degens, E T, Desai, B N and Honjo, S, *Nature*, 1989, **338**, 749–751.
23 George, M D, Kumar, M D, Naqvi, S. W A, Banerjee, S, Narvekar, P V, de Souza, S. N and Jayakumar, D A., *Mar. Chem*, 1994, **47**, 243–254.
24 Kumar, M D, Rajendran, A, Somasundar, K, Ittekkot, V. and Desai, B N, in *Oceanography of the Indian Ocean* (ed. Desai, B N). Oxford & IBH, New Delhi, 1992, pp 313–325.
25 Naqvi, S W A and Noronha, R. J, *Deep-Sea Res.*, 1991, **38**, 871–890
26 Law, C S and Owens, N. J P., *Nature*, 1990, **346**, 826–828.
27 Naqvi, S W. A, Jayakumar, D A, Nair, M., Kumar, M. D. and George, M D, *Mar Chem*, 1994, **47**, 279–290
28 Takahashi, T, *Oceanus*, 1989, **32**, 22–29
29 Tans, P P, Fung, I Y and Takahashi, T, *Science*, 1990, **247**, 1431–1438
30 Somasundar, K Rajendran, A, Kumar, M. D and Sen Gupta, R, *Mar Chem*, 1990, **30**, 363–377
31 Naqvi, S W A, Sen Gupta, R and Kumar, M. D, in *Interactions between Global Climate Subsystems, The Legacy of Hann*, Geophysical Monograph No. 75, IUGG Volume 15, American Geophysical Union, 1992, pp 85–92.
32. Pande, K., Sarin, M. M, Trivedi, J R, Krishnaswami, S and Sharma K. K, *Chem Geol*, **116**, 245–259.
33 Naqvi, S. W. A., Noronha, R J., Shailaja, M S, Somasundar, K. and Sen Gupta, R., in *Oceanography of the Indian Ocean* (ed. Desai, B. N), Oxford & IBH, New Delhi, 1992, pp 285–311
34. Safiullah, S., Mofizuddin, M., Ali, S. M. I and Kabir, S. E., in *Transport of Carbon and Minerals in Major World Rivers*, SCOPE/UNEP Sonderband Heft 64, 1987, Part 4, pp 435–442.
35. Kumar, M. D., George, M. D. and Sen Gupta, R, in *Oceanography of the Indian Ocean* (ed. Desai, B. N), Oxford & IBH, New Delhi, 1992, pp. 347–358
36. Kumar, M D, Naqvi, S. W. A, George, M. D and Jayakumar, D. A., submitted to *J Geophys. Res.*
37. Etcheto, J, Boutin, J. and Merlivat, M., *Tellus*, 1991, **43**, 247–255

ACKNOWLEDGEMENTS. We thank the Director, NIO, Dr A. P. Mitra and Dr R. Sen Gupta for their encouragement and support.

Received 2 September 1994, revised accepted 8 September 1995

RESEARCH ARTICLES

Internal waves – A novel measurement technique

Rao Tatavarti, P. N. Ananth, K. Rajasree*, V. Vidyalal*, P. Radhakrishnan*, V. P. N. Nampoori* and C. P. G. Vallabhan*

N P O L., Defence Research and Development Organization, Thrikkakara, Cochin 682 021, India
*Laser Division, International School of Photonics, Cochin University of Science and Technology, Cochin 682 022, India

We present here a novel opto-electronic technique to directly measure the internal wave oscillations, created by systematically disturbing a density stratified water column with a rotating propeller in a laboratory wave tank. The technique, based on the principle of laser beam deflection (LBD), apart from being noninvasive and highly sensitive, does not have the customary constraints on the sampling frequency and the duration of data sampling, as is the case with conventional experimental procedures. The noninvasive nature of this technique has good potential in future studies of diffusion and mixing processes in different disciplines.

INTERNAL waves in the ocean are ubiquitous, being associated with wind and air pressure fluctuations, changes in ocean floor topography, wakes of moving bodies and instabilities in the water body. Studies on internal waves enable a better understanding of the various mixing processes in the ocean, which result in the redistribution of momentum, temperature (heat) and salinity, responsible for climatic changes and, nutrients responsible for biological productivity. The oceanic internal waves occupy a vast continuum of spatial and temporal scales[1]. Available data on oceanic motions suggest horizontal scales ranging from a few tens of meters to a few kilometers and temporal scales ranging from the inertial period f^{-1} (order of magnitude in days), to the Brunt Vaisala period N^{-1} (order of magnitude in minutes).

Internal wave measurements

To the best of our knowledge, only indirect eulerian field of internal waves were measured by monitoring a closely related physical parameter like temperature or current velocity. Lagrangian field measurements of internal waves involve neutrally buoyant floats that are tracked, or sensor arrays towed horizontally through water. The literature[2–6] points out the limitations of the indirect eulerian measurements, whereas the established Lagrangian techniques are constrained by the uncertainties in understanding the underlying physics[7].

The electrical conductivity of salt water in the ocean was earlier considered to provide a convenient way of

measuring density in a stratified fluid. In this technique, the total impedance between a relatively large fixed electrode and a much smaller, movable platinum electrode is measured in an A.C. bridge network. However, two difficulties are encountered in practice. First, the probe impedance tends to drift with time. Second, time response of the probe is limited, roughly by the time required to convect material across the probe volume[8].

Remote sensing of oceanic internal waves from airborne synthetic aperture radar (SAR) imagery, a state-of-art measurement technique, involves intricate calibrations and signature extraction techniques. As the patterns on SAR imagery caused by mesoscale oceanic features are only a surface manifestation of subsurface physical processes, it is imperative to develop a robust theoretical model which links the subsurface processes to SAR-observed surface patterns. Both the manner in which SAR data are calibrated and the techniques used to extract the signatures associated with the surface patterns of interest can significantly influence the magnitude and structure of the SAR signature[9].

Laboratory investigations of internal waves primarily utilize noninvasive flow visualization techniques, as *in situ* monitoring of the complex internal wave dynamics is difficult[8]. Though flow visualization techniques give a comprehensive picture of the processes involved, they are primarily qualitative in nature. Flow visualization techniques are broadly subdivided into those that make use of light scattered by tiny particles in the fluid and those that make use of variations in the refractive index. Among the former, laser Doppler anemometry is now a standard means of obtaining fluid velocities. The fluid velocity can be measured with a high degree of accuracy as a function of time but only at a single point in the fluid at any given time[10]. Although, recent studies have shown that the instantaneous velocity field over a complete plane of interest in the fluid is now possible with speckle photography, the potential applications to fluid mechanics have not yet been fully explored.

Of the methods making use of refractive index variations, the laser beam deflection (LBD) or the mirage effect has been increasingly used in recent years for various applications[11,12], in which, the optical probe beam deflection due to an *artificially* generated refractive index gradient (RIG) is generally monitored.

Novel opto-electronic technique to monitor internal waves

Internal waves in a stratified fluid involve changes of refractive index across the field to be investigated, which may be visualized or photographed using optical methods that depend on the effects of the refractive index changes on the transmission of light. Several techniques are available of which the Schlieren techniques have been extensively used. The main use of Schlieren and direct shadow methods is to show the position and shapes of regions of density changes, such as those occurring in high speed flows, mixing problems and problems of free and forced convection.

Concept

In this section we present a novel optical technique, based on the principle of LBD, to directly quantify internal waves in the laboratory, generated by the rotating propeller of a self-propelled body submerged in a stratified water column.

In an inhomogeneous medium as in the presence of internal waves in a stratified water column, a laser beam gets deflected because of the *naturally* occurring, time-varying changes in the density of the medium (and therefore, the RIG) at a particular location. For laser beams with a gaussian intensity profile, the output voltage change monitored by a small area photo detector system is closely related to the changes in beam deflection[13]. Using this principle we were able to directly monitor internal waves generated by the rotating propeller of a stationary body placed inside a 6 mm thick perspex tank (1.8 m × 0.3 m × 0.5 m) containing an exponentially stratified salt water column.

The technique depends on the deflection of a ray of light from its undisturbed path when it passes through a medium in which there is a component of the gradient of the refractive index normal to the ray. The deflection of light ray is a measure of the first derivative of density with respect to the distance, i.e. the density gradient and therefore, it can be shown that the curvature of the ray is proportional to the refractive index gradient normal to the ray. If the Y axis is taken in the direction of the undisturbed ray, the curvatures in the XY and ZY planes respectively are given by

$$\frac{\partial^2 x}{\partial y^2} = \frac{1}{\mu}\frac{\partial \mu}{\partial x}, \qquad \frac{\partial^2 z}{\partial y^2} = \frac{1}{\mu}\frac{\partial \mu}{\partial z}. \tag{1}$$

If the total angular deflections in the XY and ZY planes are denoted by ε'_x and ε'_z respectively, then

$$\varepsilon'_x = \int \frac{1}{\mu}\frac{\partial \mu}{\partial x}\mathrm{d}y, \qquad \varepsilon'_z = \int \frac{1}{\mu}\frac{\partial \mu}{\partial z}\mathrm{d}y. \tag{2}$$

If the optical disturbance is in the working section of the wave tank, the ray of light will be deflected on leaving the tank so that

$$\mu \sin \varepsilon' = \mu_0 \sin \varepsilon, \tag{3}$$

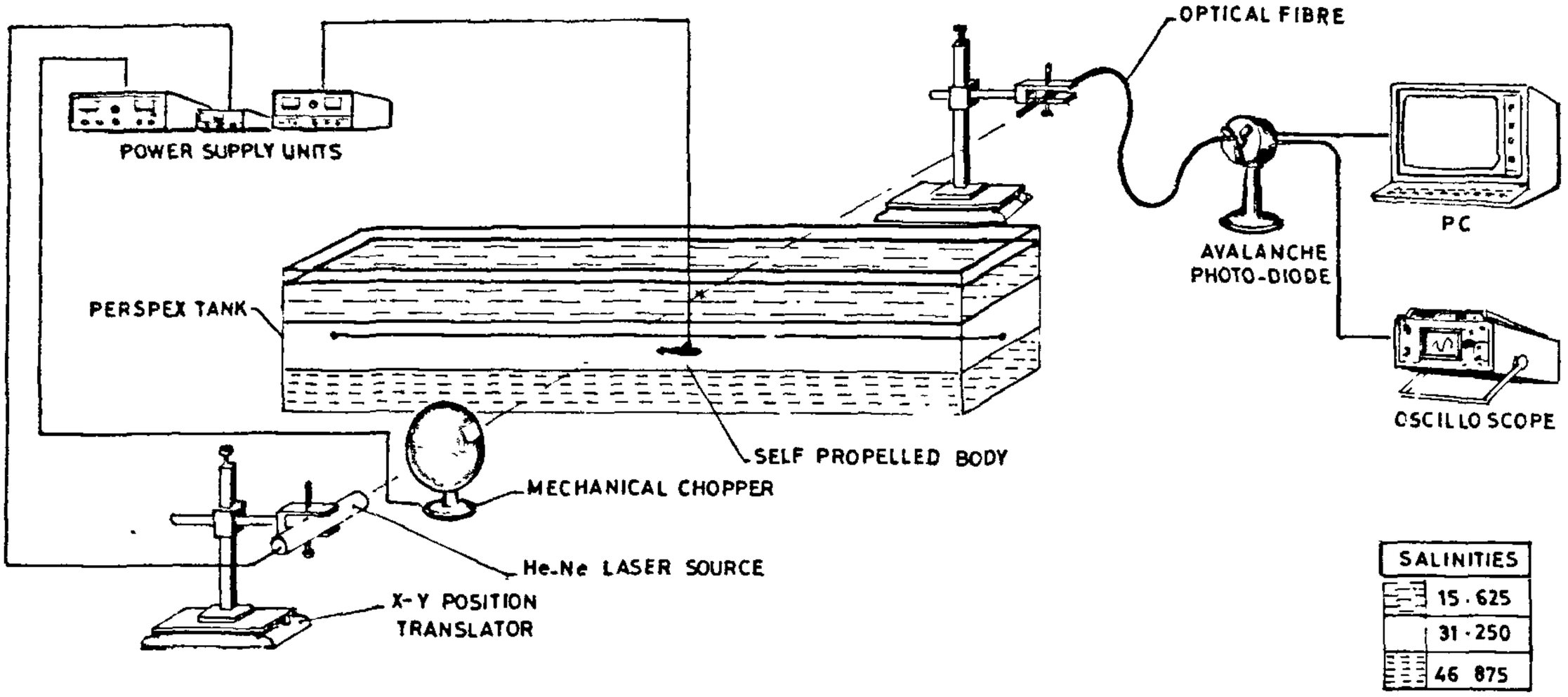

Figure 1 Schematic diagram of the experimental set-up to monitor internal waves in a stratified fluid employing the laser beam deflection technique

where μ_0 is the refractive index of the air surrounding the tank, and μ is the refractive index in the working section. Thus, the final angular deflection ε measured beyond the tank is given by

$$\varepsilon_x = \frac{1}{\mu_0}\int \frac{\partial \mu}{\partial x}\,dy, \qquad \varepsilon_z = \frac{1}{\mu_0}\int \frac{\partial \mu}{\partial z}\,dy, \tag{4}$$

where the integrals are taken over the width of the working section. In the case of two-dimensional flow in a wave tank of width L these expressions simply become

$$\varepsilon_x = \frac{L}{\mu_0}\frac{\partial \mu}{\partial x}, \qquad \varepsilon_z = \frac{L}{\mu_0}\frac{\partial \mu}{\partial z}, \tag{5}$$

the deflections being in the direction of the RIG, i.e. towards the region of higher density.

The noninvasive nature of this technique has potential application in the study of diffusion and mixing processes in different disciplines, especially biofluid mechanics. The technique can be adapted for oceanographic field applications.

Laboratory studies

Experimental set-up. An intensity stabilized 5 mw, He–Ne continuous-wave laser beam (half power beam width of 0.84 mm) was used as the probe. The deflections of the probe beam caused by the induced RIG in the medium were detected by a position sensitive detector (PSD). The polished tip of a multimode optical fibre (80/120 μm) served as the sensor head of the PSD. The other end of the optical fibre was coupled to an avalanche photodiode (APD, *Thorn EMI* make), which was incorporated into an appropriate detector circuit of very low noise level. The output voltage from the APD circuit is piped into a personal computer using a high speed analogue to digital conversion data acquisition card. The resolution of the analogue to digital voltage conversion was 0.0024414 V. As the probe beam is continuous, the sampling frequency and duration of the data sample can be chosen without any constraints. The experimental set-up is shown in Figure 1.

Prior to each experiment, a mechanical chopper placed between the laser source and the tank was used to maximize the output signal by properly aligning the probe beam and the PSD. During the actual experiments, however, the chopper was removed. Initially, experiments were carried out to ascertain that temporally and spatially varying beam deflections occur only due to changes in the RIG of the medium in the wave tank, but not due to the RIG at the air–perspex–water interfaces. Hence, the time-varying beam deflections or changes in the output voltages can be attributed to the internal wave (density) fluctuations, generated by the propeller motions of the stationary body inside the stratified water column.

Calibrations. Utilizing known density samples in the perspex tank, the output voltages of the laser beam propagating through the samples were monitored. An output voltage of 3.62 V was observed for a sample density of 1.0043 g/cc and an output voltage of 1.08 V

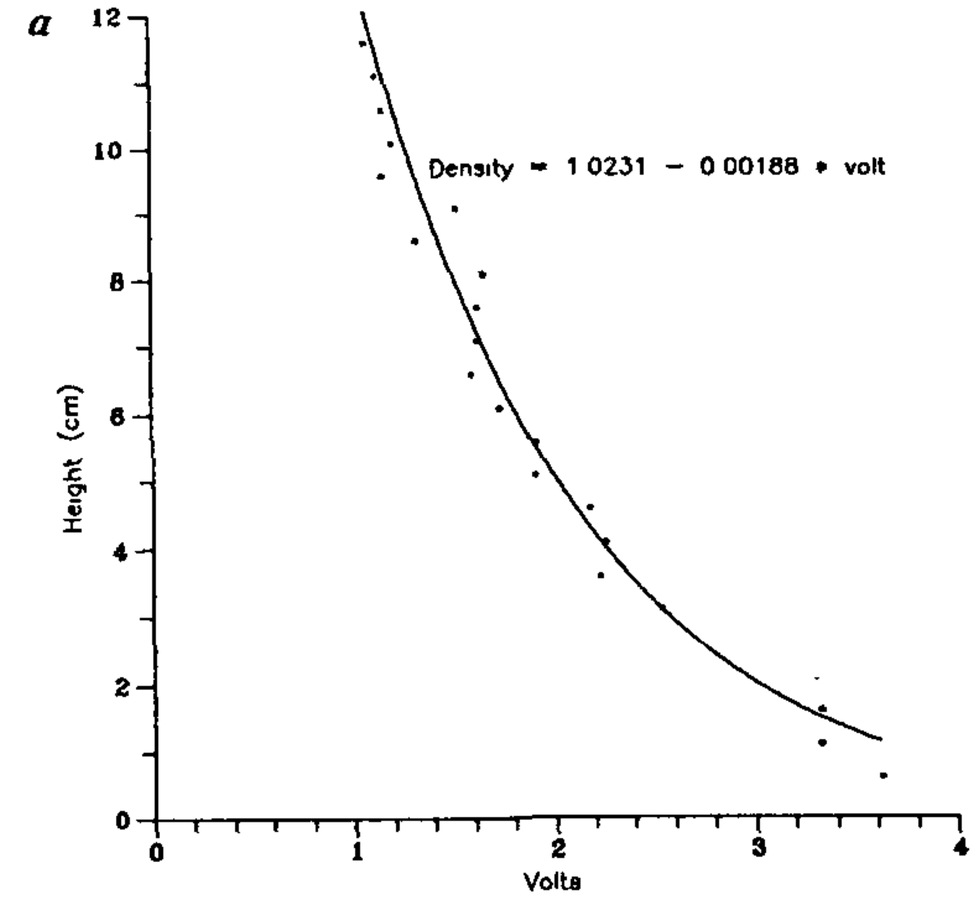

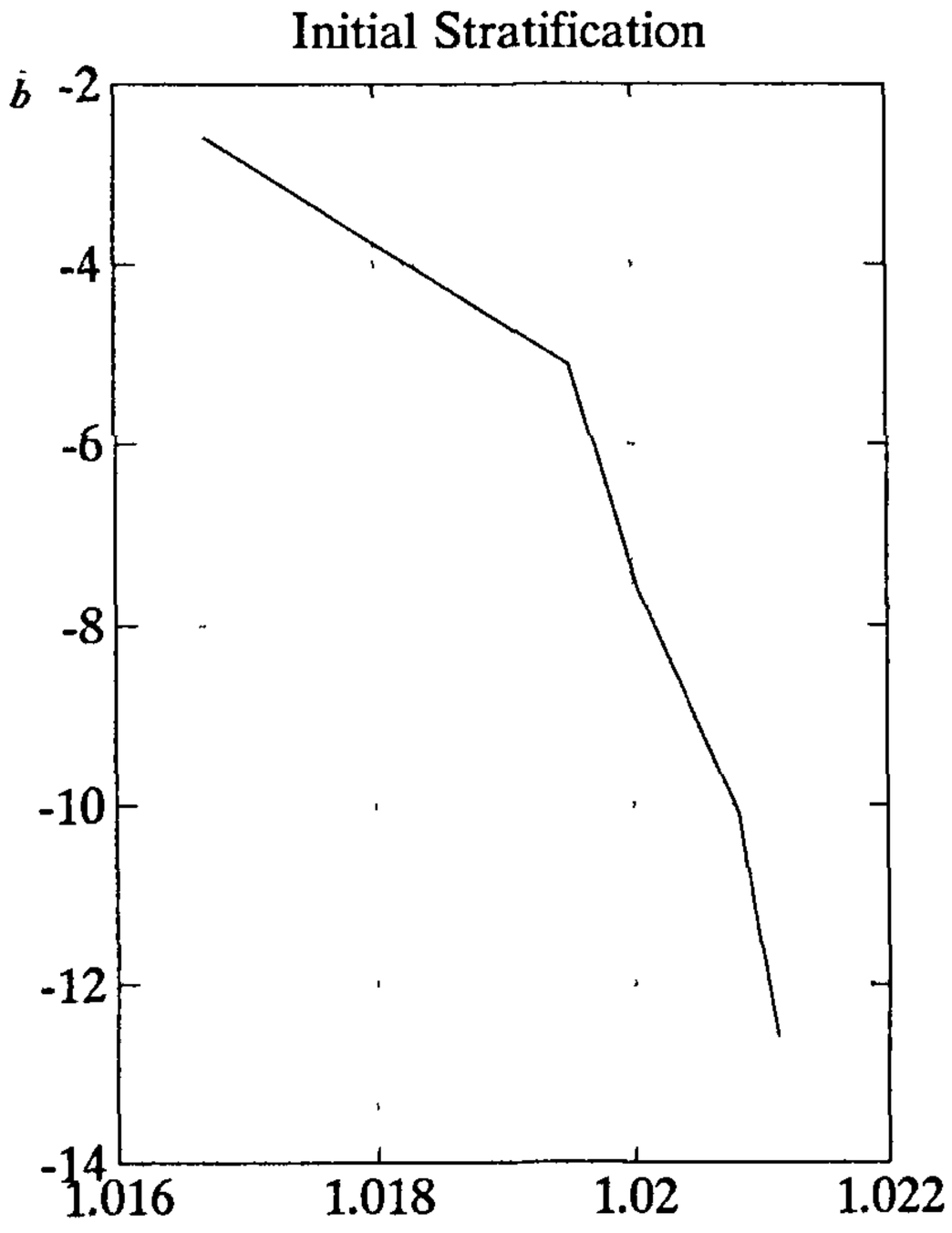

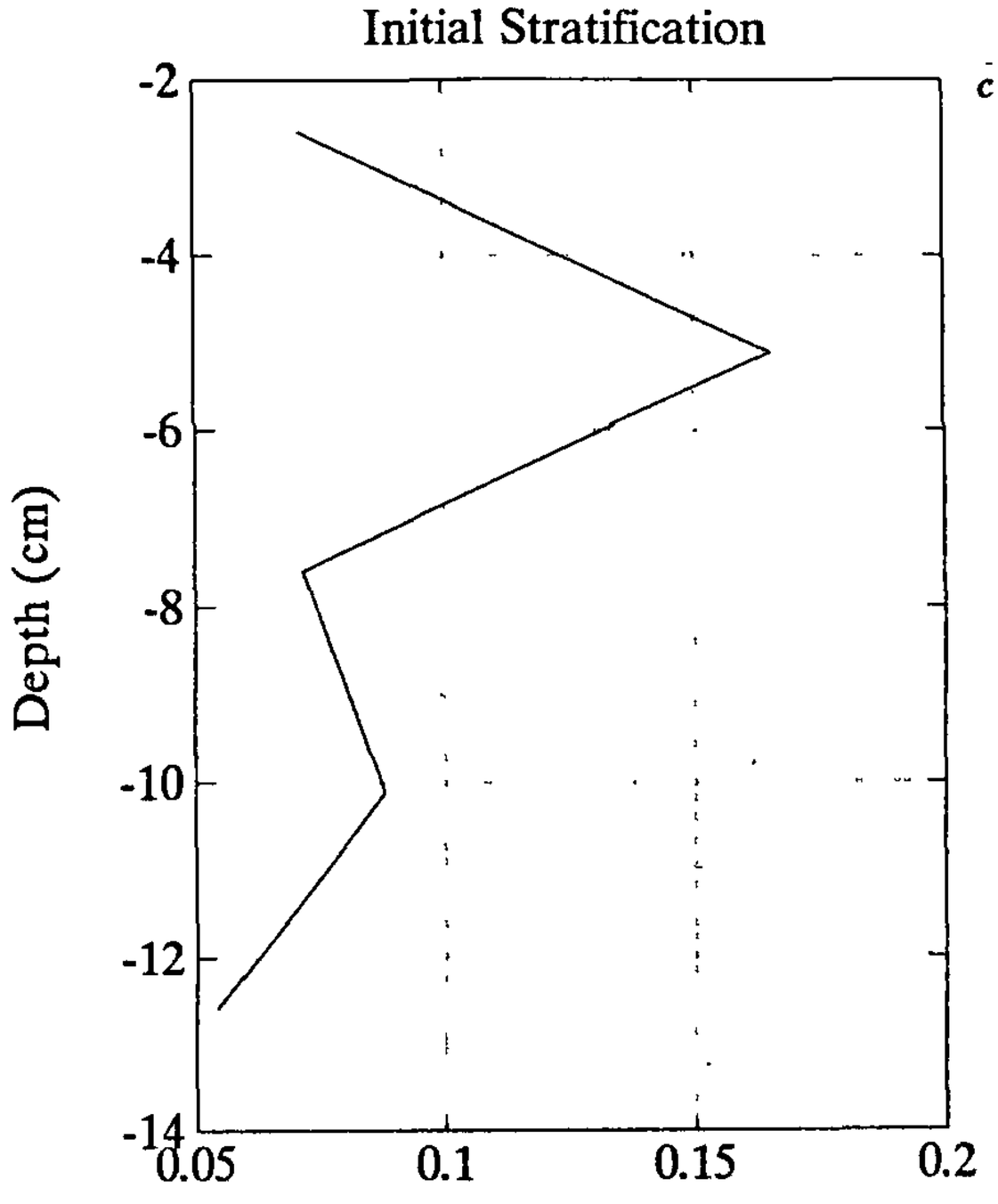

Figure 2 Initial output voltage distribution (*a*), calibrated density stratification (*b*), and the associated Brunt-Vaisala frequency [$N(z)$] profile (*c*), in the laboratory tank before the start of the experiment, where $N^2(z) = g/\rho_o\{\partial\rho/\partial z\}$.

was observed for a sample density of 1.0231 g/cc. Initially, a step-distribution was obtained by sequentially introducing the bottom layer (1.0231 g/cc), the middle layer (1.0113 g/cc) and the top layer (1.0043 g/cc) into the tank. Before introducing the middle and top layers, a wax paper was stretched on top of the water in the tank and the next layer added, after which the wax paper was rolled up from one end of the tank ensuring minimal disturbance. Molecular diffusion was allowed to take place for about a day, which resulted in the exponential distribution.

The output voltages of the laser beam propagating at different levels of the tank, in the vertical direction were monitored. Figure 2 *a* shows the vertical profile of output

voltages approximately a day after introducing the three layers in the tank. The exponential distribution is an artifact of the molecular diffusion. The calibration constants were obtained after solving the simultaneous (straight line) equations relating density and voltage. The gain and offset calibration constants were found to be 0.00188 and 1.0231 respectively. Figures 2 *b* and 2 *c* show the corresponding density and Brunt-Vaisala distributions in the tank. The output voltage from the APD circuitry which is piped into the PC as digital data is finally calibrated as density fluctuations.

Experiments. At the start of each experimental run the propeller was switched on. The sampling frequency was chosen as 100 Hz. In order to avoid reflections from the end walls of the tank, the duration of sampling for each run was limited to 2 min, the monitored travel times of hydrodynamical signatures from source to the end wall being greater than 2 min. Four major experiments covering 80 data runs in total were conducted with the laser source-detector system and the stationary body with its rotating propeller placed at different positions, for the same stratification. Detailed studies on different aspects of internal wave dynamics and mixing are being reported elsewhere. In this article, however, we present data from one of the typical experiments. During this experiment, time series observations of density fluctuations were monitored at 24 different locations along the wall of the tank forming a vertical array of time series observations as shown in Figure 3. In this article, however, data from the first vertical array of observations are only being reported. For all the observations, the position of the stationary body with its rotating propeller was fixed and only the position of the laser source-detector system was varied. Before each observational run, the propeller was switched on and after each observational run of 2 min duration, the propeller was switched off, allowing the water to settle down to its equilibrium position. As the forcing imparted to the water inside the tank was not strong (just sufficient to create internal wave fluctuations only) it is assumed that the mixing created by propulsion of the stationary body does not alter the characteristics of the stratified water column in the tank in a significant manner. The wake generated by a submerged body moving through a density-stratified medium is a turbulent region of mixed fluid of homogeneous density. The observations of earlier researchers that due to the stabilizing effect of the stratification, turbulence near the wake boundary is rapidly damped and does not cause appreciable mixing of the fluid with its surroundings, give ample support to our assumption. Therefore, as the mixed fluid seeks to return to its equivalent density level, the region collapses vertically and internal waves are consequently generated. At each location, the mean density value obtained during calibration experiment was deducted from the time series observations at that location to ensure that the observations reflect the actual density fluctuations caused by internal wave dynamics.

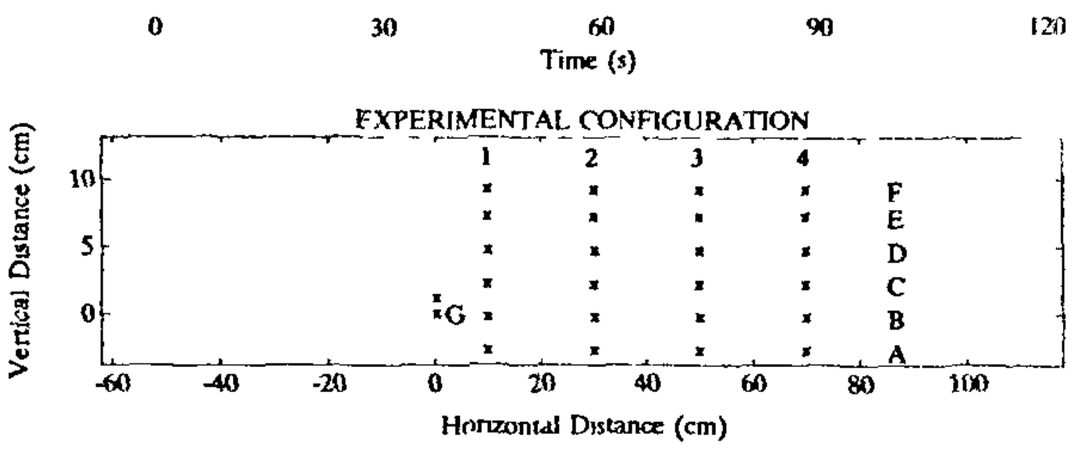

Figure 3. Experimental configuration The crosses denote the exact locations where measurements were made. The *X*-direction is denoted by 1, 2, 3 and 4. The *Z*-direction is denoted by A, B, C, D, E and F. The propeller (origin) was lying 0.5 cm to the left of G

Conventional Schlieren techniques – Limitations

Our technique is similar in principle to the Schlieren system[14,15]. However, the primary difference is that a conventional Schlieren system enables only qualitative flow visualization based on frame-to-frame observations, whereas our technique provides quantitative point-probe diagnostics continuously.

Conventional Schlieren techniques tend to become ineffective in monitoring smaller density changes of a medium. Indeed, when the density changes are very low (as in our study), conventional Schlieren methods can no longer be used as there is a progressive loss of contrast in the records that cannot be overcome by any normal modification to the apparatus or in the photographic processing.

In addition to limitations to the dimensions of mirrors and lenses used in conventional Schlieren techniques, the effects of diffraction may result in a change of illumination on the viewing screen, which differs appreciably in both extent and magnitude from that expected on the basis of geometrical optics. These effects may considerably affect the accuracy of the Schlieren technique when used to quantify density variations.

Even when high-speed cine cameras are used to quantify complicated dynamical processes (like internal waves in stratified fluid), the picture sharpness is usually less satisfactory in a direction along the film than across it[16].

Toepler–Schlieren photography can only offer the phase configurations, but our technique can determine the amplitude and phase of the signature using standard signal processing techniques. Moreover, the fact that none of the limitations associated with conventional Schlieren techniques arise when internal waves are monitored using the present method justifies that the technique reported here is more effective and sensitive.

Results and discussion

Typical time series plots of the density fluctuations, i.e. the raw data, along with a plot depicting the noise in

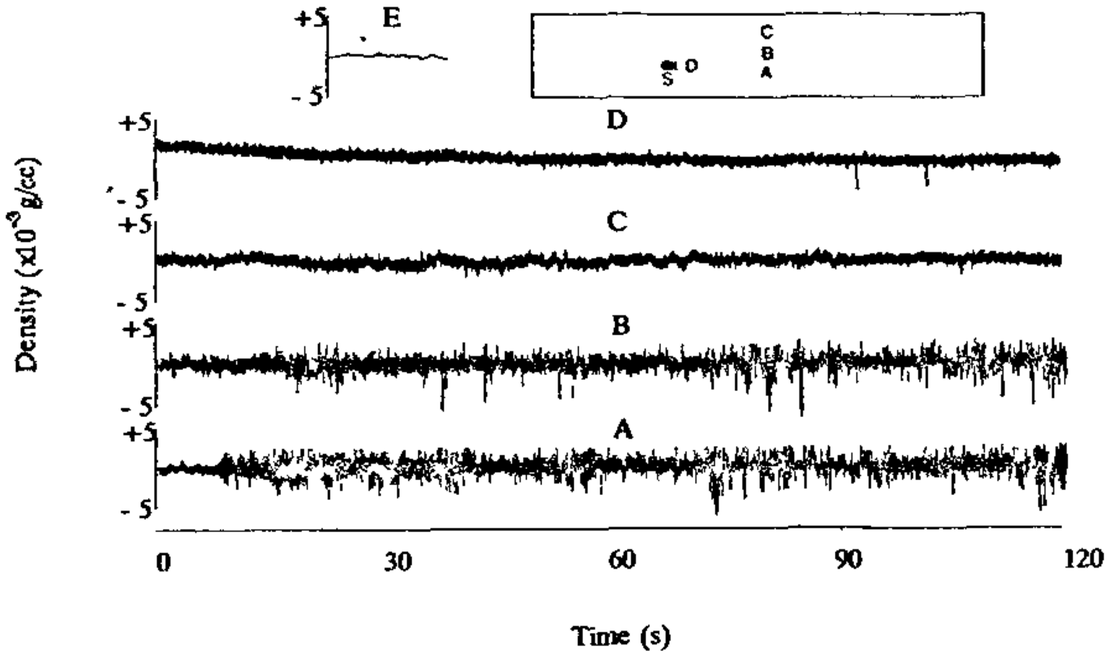

Figure 4 Time series of the observed density fluctuations caused by the turbulent wake and internal waves at different vertical locations A, B, C, D. Data run E depicts the ambient noise level at the location of A when the propeller was inoperative Inset is a schematic diagram showing locations of runs A, B, C, D and the body S.

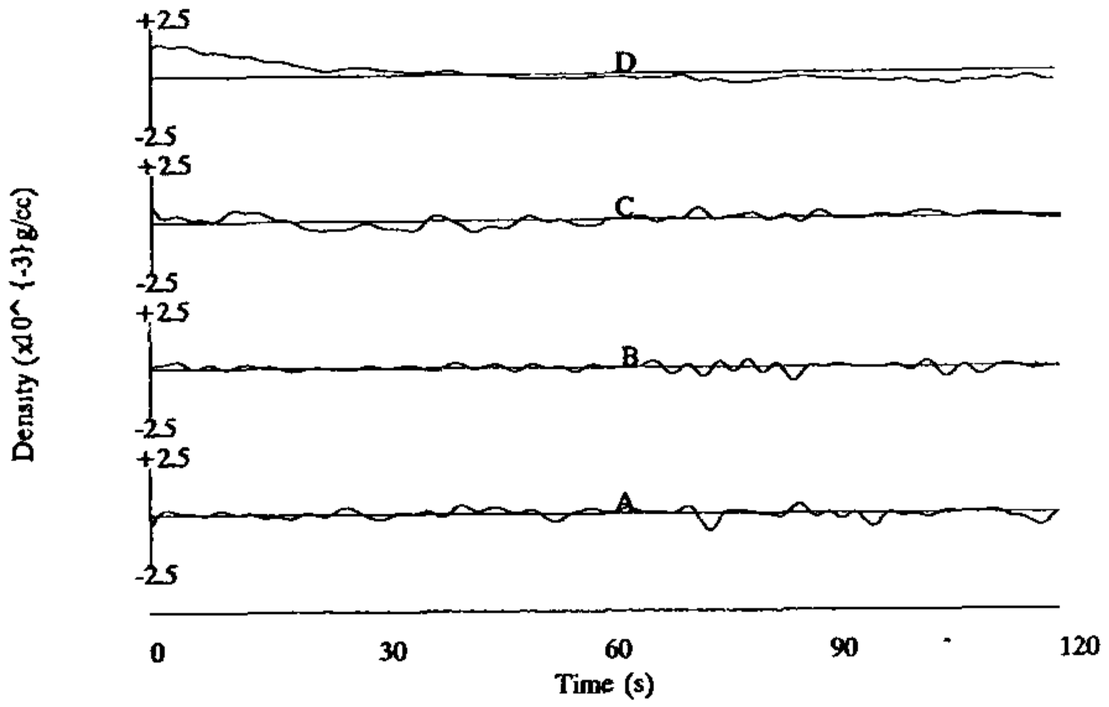

Figure 5. Time series of the low passed density fluctuations at different vertical locations. The data are the same as those shown in Figure 4

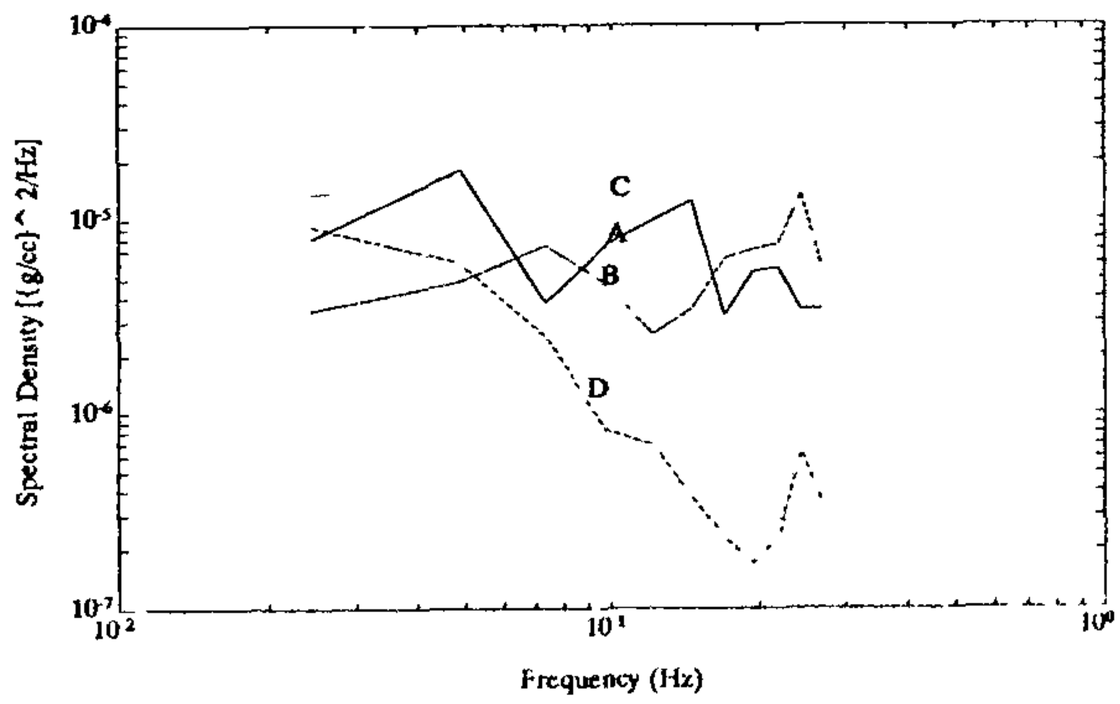

Figure 6 Spectral densities of the low passed density fluctuations recorded at different vertical locations A, B, C, D. The units on Y-axis are $[(g/cc)^2/Hz]$ Frequency resolution is 0 0244 Hz Degrees of freedom ≅ 10

measurements (i.e. when the signatures were observed while the water in the tank was undisturbed, the propeller being stationary) are shown in Figure 4. Two inferences become evident from Figure 4. One, the amplitudes of

Table 1. Wavenumber k_x (values in rad/cm)

	Horizontal distance (cm)					
	10 –30	30 –50	50 –70	10 –30	30 – 50	50 – 70
	Frequency = 0 0244 Hz			Frequency = 0 1465 Hz		
F	–0 030	0 147	–0 138	0.102	0 143	–0.044
E	–0.206	0.199	–0 232	0 211	–0.256	0 142
D	0.208	0 031	–0 267	0.239	–0.022	–0.095
C	–0.212	0 007	0 030	0.110	–0.098	0.109
B	–0 049	0 069	–0 018	0.008	–0.470	–0.045
A	–0 259	0 190	0 074	0 158	–0 071	0 067

The origin of the horizontal distances is the source of forcing.
A – F denote vertical locations separated by 2.5 cm.

the fluctuations are small, indicating the minimal forcing applied on the propeller of the stationary body to avoid reflections and significant mixing; and two, the technique is very sensitive having minimal noise as can be seen in the uppermost plot of Figure 4. The maximum Brunt-Väisala frequency for our stratification was of the order of 0.2 Hz as reported earlier. Hence, the raw time series data were low passed using a Chebyshev filter with a cut-off frequency at 0.2 Hz to remove extraneous signatures, presumably associated with nonlinearities and turbulence, from analysis of internal wave dynamics. However, it may be noted that the detector does not yield any output corresponding to that part of the turbulence which does not induce any change in RIG in the medium. Figure 5 shows some typical time series plots of the low passed density fluctuations considered in the present study. Spectral density plots of the low passed raw data are shown in Figure 6. Spectral computations were performed using a Hanning window with 50% overlap. The spectral estimates have approximately 10 degrees of freedom with a frequency resolution of 0.0244 Hz. The spectral observations have been resolved into eight frequency bands. Significant spectral energy levels at different frequency bands can be observed in Figure 6.

Tables 1 and 2 show the scalar wavenumbers, corresponding to two frequencies in the internal wave band, computed as $k_x = \Delta\phi_x/\Delta x$, and $k_z = \Delta\phi_z/\Delta z$, where k_x is the horizontal wavenumber in the X-direction and k_z is the vertical wavenumber in the Z-direction and $\Delta\phi_x$, $\Delta\phi_z$ are the autospectral phase differences in the respective X and Z directions. Although k_x and k_z computations do not correspond to the same location, they do suggest that those in the X-direction are of an order of magnitude less than those in the Z-direction. This is consistent with the laboratory set up of a vertically stratified water column in the wave tank, which inhibits propagation in the vertical. As a result, the spatially inhomogeneous turbulence undergoes a transition to two-dimensional motion under the action of stratification, and there would be a propensity for a stronger horizontal propagation, as suggested by the recent stratified shear flow experiments[17,18].

However, the basic observations which suggest that turbulence dominates in the near field of the source and

Table 2 Wavenumber k_z (values in rad/cm)

	Horizontal distance (cm)							
	10	30	50	70	10	30	50	70
	Frequency = 0 0244 Hz				Frequency = 0 1465 Hz			
E–F	2 001	0 107	0.517	–0 231	0 379	1 255	–1.937	–0 446
D–E	–1 785	1 531	0.187	–0 094	–0 624	–0 401	1 473	–0 427
C–D	1 606	–1 757	–1 944	0 427	1 292	0 259	–0 345	1 288
B–C	–0 004	1 303	1 795	1 412	–0 273	–1 091	–0 685	–1 917
A–B	0 221	–1 463	–0 490	0 251	–0 941	0 266	0 073	0 968

The origin of the horizontal distances is the source of forcing.
A–F denote vertical locations separated by 2.5 cm.

internal waves generated by the collapse of the turbulent wake dominate in the far field (see the raw time series plots in Figure 4 and low passed plots in Figure 5) are consistent with earlier studies[19,20]. Close to the centre of the disturbance, internal waves generated due to the displacement effects of the propeller propagate in a narrow region along the axis of the generating source[21]. This feature is reflected in the time series plots of run D.

The spectral observations in Figure 6 show that near the source (runs A & B), turbulence manifests (broad band spectra) and along the axis of the source (run D), internal wave signatures manifest as higher energy in the lower frequencies of the spectra, rapidly decaying towards higher frequencies. The spectral peaks associated with different frequencies at different locations are indicative of the multiple interactions between various components creating nonlinear energy transfers[22,23].

Conclusions

A novel optoelectronic technique to directly monitor internal waves in the laboratory was demonstrated. The technique is highly sensitive and is free from the conventional experimental constraints. It can be easily adapted for use in field experiments.

1. Garrett, C. J R. and Munk, W., *Geophys. Fluid Dyn*, 1975, **2**, 225–264
2. Woods, J. D., *J. Fluid Mech*, 1968, **32**, 791–800.
3 Wunsch, C., *J. Geophys Res.*, 1975, **80**, 339–343.
4 Katz, E. J, *J Phys Oceanogr*, 1973, **3**, 448–457.
5 Cairns, J. L, *J. Geophys. Res*, 1975, **80**, 299–306.
6. Bell, T. H, *J. Geophys. Res.*, 1976, **81**, 3709–3714.
7. Müller, P., Olbers, D J. and Willebrand, J., *J Geophys. Res*, 1978, **83**, 479–500.
8. Maxworthy, T. and Browand, F. K., *Annu. Rev Fluid Mech*, 1975, **7**, 273–305.
9. Kasischke, E. R, *IEEE J. Oceanic Engg*, 1990, **15**, 126–130
10. Lauterborn, W. and Vogel, A., *Annu. Rev. Fluid Mech*, 1984, **16**, 223–244.
11. Sell, J. A., *Photo Thermal Investigations of Solids and Liquids*, Academic Press, London, 1989.
12. Rajasree, K., Vidyalal, V., Radhakrishnan, P., Nampoori, V P. N. and Vallabhan, C. P. G, *Meas Sci. Technol*, 1992, **4**, 435–437.
13. Mandells, A., Takaue, R, Chen, Z, Szurmak, J and Baines, W. D, *Anal. Sci*, 1992, **8**, 131–136.
14. Mowbray, D E. and Rarity, B S., *J. Fluid Mech.*, 1976, **28**, 1–16.
15. Stevenson, T. N., *J. Fluid Mech.*, 1973, **60**, 759–767.
16. Holder, D. W. and North, R. J, *Schlieren Methods*, A National Physical Laboratory Publication, Middlesex, UK, 1963.
17. Lighthill, J., in *Waves in Fluids*, Cambridge University Press, London, 1978, p. 505.
18. Chu, V. H. and Baddour, R. E., *J. Fluid Mech*, 1984, **138**, 353–379.
19 Schooley, A. H. and Steward, R. W., *J. Fluid Mech*, 1963, **15**, 83.
20 Wu, J, *J. Fluid Mech*, 1969, **35**, 531–544
21. Sherman, F. S., Imberger, J. and Corcos, G. M, *Annu Rev. Fluid Mech*, 1978, **10**, 267–288.
22 Martin, S, Simmons, W. F. and Wunsch, C. I., *J Fluid Mech*, 1972, **53**, 17–44.
23. McEwan, A. D. and Robinson, R. M, *J. Fluid Mech*, 1975, **67**, 667–687.

ACKNOWLEDGEMENTS. Assistance from T. P. Muralidharan, NPOL is gratefully acknowledged KR and VV thank UGC and CSIR for their research fellowships. PR, VPNN and CPGV thank MHRD, Govt of India for financial grant. RT and PNA thank Director, NPOL for the encouragement and facilities provided.

Received 7 October 1994; revised accepted 26 September 1995